The impact of nuclear reactions on the neutron-star g-mode spectrum

A. R. Counsell ⬤,★ F. Gittins ⬤ and N. Andersson ⬤
Mathematical Sciences and STAG Research Centre, University of Southampton, Southampton, SO17 1BJ, UK

ABSTRACT

Mature neutron stars are expected to exhibit gravity g modes due to stratification caused by a varying matter composition. These modes are affected by nuclear reactions, leading to complex (damped) mode frequencies and the suppression of high-order g modes. This is in contrast with the common non-dissipative analysis which leads to an infinite g-mode spectrum. Focusing on the transition between the fast- and slow-reaction regimes, we examine the precise impact of nuclear reactions on the g-mode spectrum. The general framework for the analysis is presented along with sample numerical results for a matter model based on the BSk21 equation of state with a suitable parametrization for the reaction rates.

Key words: stars: interiors – stars: neutron – stars: oscillations.

1 INTRODUCTION

Neutron stars are highly compact objects that involve a rich and complex variety of physics. Due to this, there are (more or less) specific classes of oscillation modes associated with each aspect of the physics involved. One key feature is the varying composition of matter, introducing buoyancy as a restoring force in the equations of fluid dynamics (Reisenegger & Goldreich 1992). This, in turn, leads to the presence of low-frequency gravity g modes. The typical frequency of the leading neutron star g mode is of the order of a few 100 Hz (depending on the matter equation of state) and the higher overtones lie at lower frequencies. As these modes rely on stable composition stratification for their existence, they are sensitive to nuclear reactions. Reactions will strive to reinstate beta equilibrium in the neutron star matter and hence lead to each g mode becoming damped. This description is really only relevant in the limit of infinitely slow nuclear reactions. While it may apply to the highest frequency g modes (the lowest overtones) there will always be modes (likely very high overtones) that have low enough frequency that the impact of finite nuclear reactions must be accounted for (Andersson & Pnigouras 2019). Hence, it is interesting – at least from a conceptual point of view – to consider the impact of nuclear reactions on the g-mode spectrum. This is the issue we explore in the following. The aim is to establish a more precise understanding of how the g modes are affected by reactions and what happens to the mode spectrum when the reaction rate becomes fast compared to the dynamics.

The importance of stellar seismology has been appreciated since the work of Cowling (1941) (see Cox 1980; Unno et al. 1989). While originally the focus was on the mathematical formulation of the problem, recent X-ray timing observations and the detection of gravitational waves from the GW170817 neutron star merger event have led to renewed focus on the problem (Abbott et al. 2017, 2018).

The vast majority of the literature on neutron star seismology has focused on oscillation modes that depend weakly on the precise nuclear physics below the crust, such as the fundamental f mode or the pressure p modes. Moreover, due to the complexity of the problem, different aspects of the physics is commonly studied one piece at a time.

A considerable body of work has been dedicated to the neutron star g modes (see McDermott, van Horn & Scholl 1983; Finn 1986; Miniutti et al. 2003, to name a few). This is natural, as these modes should be present in both mature and hot young neutron stars (noting recent evidence that the g modes may be excited during the proto-neutron star stage following a core-collapse supernova; Vartanyan et al. 2023). In general, the g modes depend on both the internal matter composition and the state of matter (e.g. the presence of neutron superfluidity; Passamonti, Andersson & Pnigouras 2022). Unlike other oscillation modes such as the f and p modes, the g modes rely specifically on the conditions in the outer core of a neutron star, below the elastic crust. It is therefore of interest to ask what constraints on the nuclear physics could be made from stellar observations of g modes. Specifically, for a mature neutron star the mode frequencies depend on the variation of the lepton fraction with density (and the state of matter; Kantor & Gusakov 2014), in turn subject to nuclear parameters like the nuclear symmetry energy. An observation of a specific g-mode frequency – perhaps as a tidal resonance induced during binary inspiral (Andersson & Ho 2018; Ho & Andersson 2023) – might then provide some insight into the nuclear physics and the equation of state beyond bulk properties like the mass and radius of the star.

Building on the proof-of-principle work by Andersson & Pnigouras (2019), this paper considers the spectrum of g modes in a cold mature neutron star and the impact nuclear reactions have on the damping of oscillations. This is an important step as it goes beyond the plane-wave analysis from Andersson & Pnigouras (2019), accounting for the relevant mode boundary conditions and implementing the local damping associated with nuclear reactions directly. At the same time, one has to appreciate two simple facts.

★ E-mail: arc1n21@soton.ac.uk

First, as already mentioned, the reaction time–scales expected in a mature neutron star tend to be many orders of magnitude slower than the time–scale of the modes. A typical low-order g mode would have a frequency of around 100 Hz, while the modified Urca reactions act on a time–scale of (Haensel, Levenfish & Yakovlev 2002)

$$t_R \sim 10^{13} \left(\frac{10^8 \mathrm{K}}{T} \right)^6 \mathrm{s} .$$ (1)

Clearly, the neutron star matter will tend to be in the slow-reaction regime. The second fact concerns the numerical determination of low-frequency modes. It is well-known that the high-order g modes are difficult to obtain numerically. This leaves us with a conundrum: How can we gain insight into the nature of the high-order modes that are expected to be impacted by the reactions? The natural resolution is to be pragmatic. Instead of focusing on either the fast- or slow-reaction regimes, we consider how the low-order modes (which are accessible numerically) behave for arbitrary (suitably parametrized and vastly exaggerated) reaction rates and examine the effect damping has on the crossover from slow to fast reactions. This provides an understanding of the phenomenology of the problem and an idea of what happens to the very high-order g modes in a realistic neutron star model. Our demonstrations are based on a specific equation of state, BSk21 (Fantina et al. 2013; Potekhin et al. 2013), which allows us to employ a realistic description of the matter stratification. While the same information can be extracted from many other 'realistic' equation of state models, the BSk family has the advantage of being expressed in closed form, which means that the thermodynamical derivatives required for the g-mode calculation do not have to be worked out numerically. This is convenient as it avoids the numerical errors that would be unavoidable if we were to work out these derivatives from tabulated equation of state data.

The layout of the paper is as follows: in Section 2, we outline the background equations and physics that go into the problem. Section 3 examines the fast and slow reaction regimes using a plane-wave approach. Section 4 then solves the mode-problem for a general reaction rate, presenting the dimensionless equations and results. Finally, Section 5 summarizes the work and presents ideas for future continuation of this effort.

2 THE PERTURBATION PROBLEM

Even though we are ultimately aiming for realism, we will explore the impact of nuclear reactions on the g modes of a stratified neutron star in the context of Newtonian gravity. This makes the results somewhat phenomenological, but – as we have to (vastly) exaggerate the reaction rates in order to demonstrate the features we are interested in anyway – this lack of precision is not a great concern. Given this context, we consider the problem for non-rotating stars, assuming that the oscillation modes – with label n and frequency ω_n – are associated with a polar perturbation displacement vector (expressed in the coordinate basis associated with the spherical polar coordinates $[r, \theta, \varphi]$)

$$\xi_n^i(t, r, \theta, \varphi) = \xi^i(r, \theta, \varphi) e^{i\omega_n t} ,$$ (2)

with

$$\xi^i = \frac{1}{r} W_l Y_l^m \delta_r^i + \frac{1}{r^2} V_l \partial_\theta Y_l^m \delta_\theta^i + \frac{im}{r^2 \sin^2\theta} V_l Y_l^m \delta_\varphi^i ,$$ (3)

where the multipole amplitudes, W_l and V_l, are functions of r only and $Y_l^m(\theta, \varphi)$ are the usual spherical harmonics. Along with this, all scalar perturbations are expanded in spherical harmonics. That is, using δ to indicate an Eulerian perturbation, we have the perturbed

mass density

$$\delta\rho_n = \delta\rho(r, \theta, \varphi) e^{i\omega_n t} ,$$ (4)

with

$$\delta\rho = \delta\rho_l Y_l^m ,$$ (5)

and similar for all other scalar quantities. In the following, whenever p, ρ, Φ are used without δ they refer to the value of the pressure, density and gravitational potential, respectively, of the background equilibrium star. As we are ignoring rotation, the background configuration is spherical so all associated quantities are only functions of r.

Turning to the perturbed Euler equation, we have

$$-\omega_n^2 \xi_i + \nabla_i \delta\Phi + \frac{1}{\rho} \nabla_i \delta p - \frac{1}{\rho^2} \delta\rho \nabla_i p = 0 .$$ (6)

This leads to the radial component

$$\frac{d\delta p_l}{dr} - \left(\frac{\delta\rho_l}{\rho} \right) \frac{dp}{dr} = \frac{\omega_n^2 \rho}{r} W_l - \rho \frac{d\delta\Phi_l}{dr} ,$$ (7)

and then, from the φ component of the Euler equation, we get

$$\omega_n^2 V_l = \delta\Phi_l + \frac{\delta p_l}{\rho} .$$ (8)

We also need the perturbed continuity equation,

$$\delta\rho_l = -\frac{W_l}{r} \frac{d\rho}{dr} - \frac{\rho}{r^2} \left[\frac{d(rW_l)}{dr} - l(l+1)V_l \right] .$$ (9)

Combining the last two equations, we get

$$\frac{d(rW_l)}{dr} + \frac{rW_l}{\rho} \frac{d\rho}{dr} = -\frac{r^2}{\rho} \delta\rho_l + \frac{l(l+1)}{\omega_n^2} \left(\delta\Phi_l + \frac{\delta p_l}{\rho} \right) .$$ (10)

Lastly, we have the perturbed Poisson equation,

$$\nabla^2 \delta\Phi = 4\pi G \delta\rho .$$ (11)

Let us now add nuclear reactions to the problem. As the moving fluid is no longer in equilibrium, we need to consider additional parameters in the (perturbed) equation of state. A natural option, which helps account for nuclear reactions driven by the deviation from beta equilibrium, is to introduce the new variable $\beta = \mu_n - \mu_p - \mu_e$ depending on the chemical potentials for neutrons, protons, and electrons (labelled n, p, and e, respectively). In (cold) equilibrium, we then have $\beta = 0$. This condition allows us to solve for the matter composition, e.g. the lepton/proton fraction x_p for a given mass density. For simplicity, we assume pure npe matter and that the star is cold enough to be transparent to neutrinos so the relevant reactions will be the Urca reactions. However, as we have already explained, the actual reaction rates are far too slow (at least for the temperatures we have in mind) to have significant impact on the low-order g modes. Hence, we focus our attention on a parametrized mode and a wide range of reaction rates. While this means that the numerical results we obtain are, inevitably, phenomenological we believe the behaviour is robust enough that an extrapolation to realistic reaction rates/high-order modes is straightforward.[1]

We assume that the equation of state is a two parameter function $p = p(\rho, x_p)$ where x_p is the proton fraction. From Andersson & Pnigouras (2019) we have,

$$\Delta\beta = \frac{\mathcal{B}}{1 + i\mathcal{A}/\omega_n} \Delta\rho ,$$ (12)

[1] The clear agreement between the numerical results and the plane-wave analysis provides convincing support for this.

where Δ is the Lagrangian perturbation,

$$\mathcal{B} = \left(\frac{\partial \beta}{\partial \rho}\right)_{x_{\mathrm{p}}} , \tag{13}$$

and

$$\mathcal{A} = -\frac{1}{t_{\mathrm{R}}} , \tag{14}$$

where t_{R} is the characteristic reaction time (and the minus sign is a convention). Note that this means that $\Delta \beta = 0$ in the limit of very fast reactions, when $t_{\mathrm{R}} \to 0$. In the opposite limit, when reactions are slow, we have $t_{\mathrm{R}} \to \infty$ and therefore $\mathcal{A} \to 0$ and the matter composition is frozen. Moreover, given that the unperturbed star is assumed to be in chemical equilibrium we have $\Delta \beta = \delta \beta$. Using this and combining (12) and (9) we get,

$$i\omega_n \delta\beta_l - \mathcal{A}\delta\beta_l = -i\omega_n \frac{\rho \mathcal{B}}{r^2} \left[\frac{\mathrm{d}(rW_l)}{\mathrm{d}r} - l(l+1)V_l\right] . \tag{15}$$

As it is common to work with the perturbed pressure, we rewrite this equation as

$$i\omega_n \delta\beta_l - \mathcal{A}\delta\beta_l = i\omega_n \mathcal{B} \left(\delta\rho_l + \frac{W_l}{r}\frac{\mathrm{d}\rho}{\mathrm{d}r}\right) . \tag{16}$$

We also need

$$\delta p_l = \left(\frac{\partial p}{\partial \rho}\right)_\beta \delta\rho_l + \left(\frac{\partial p}{\partial \beta}\right)_\rho \delta\beta_l , \tag{17}$$

leading to

$$\delta p_l = \left[\left(\frac{\partial p}{\partial \rho}\right)_\beta + \frac{1}{1 + i\mathcal{A}/\omega_n}\left(\frac{\partial \beta}{\partial \rho}\right)_{x_{\mathrm{p}}}\left(\frac{\partial p}{\partial \beta}\right)_\rho\right]\delta\rho_l$$
$$+ \frac{1}{1 + i\mathcal{A}/\omega_n}\left(\frac{\partial \beta}{\partial \rho}\right)_{x_{\mathrm{p}}}\left(\frac{\partial p}{\partial \beta}\right)_\rho\left(\frac{W_l}{r}\frac{\mathrm{d}\rho}{\mathrm{d}r}\right) . \tag{18}$$

At this point it make sense to use the thermodynamic relation,

$$\left(\frac{\partial p}{\partial \beta}\right)_\rho\left(\frac{\partial \beta}{\partial \rho}\right)_{x_{\mathrm{p}}} = \left(\frac{\partial p}{\partial \rho}\right)_{x_{\mathrm{p}}} - \left(\frac{\partial p}{\partial \rho}\right)_\beta , \tag{19}$$

to get

$$\delta p_l = \left\{1 + \frac{1}{1 + i\mathcal{A}/\omega_n}\left[\left(\frac{\partial p}{\partial \rho}\right)_\beta^{-1}\left(\frac{\partial p}{\partial \rho}\right)_{x_{\mathrm{p}}} - 1\right]\right\}\left(\frac{\partial p}{\partial \rho}\right)_\beta \delta\rho_l$$
$$+ \frac{1}{1 + i\mathcal{A}/\omega_n}\left[\left(\frac{\partial p}{\partial \rho}\right)_\beta^{-1}\left(\frac{\partial p}{\partial \rho}\right)_{x_{\mathrm{p}}} - 1\right]$$
$$\times \left(\frac{\partial p}{\partial \rho}\right)_\beta\left(\frac{W_l}{r}\frac{\mathrm{d}\rho}{\mathrm{d}r}\right) . \tag{20}$$

Next we define the speed of sound in equilibrium and at fixed proton fraction, respectively;

$$c_{\mathrm{s}}^2 = \left(\frac{\partial p}{\partial \rho}\right)_\beta , \tag{21}$$

$$\mathcal{C}^2 = \left(\frac{\partial p}{\partial \rho}\right)_{x_{\mathrm{p}}} . \tag{22}$$

These quantities are related to the commonly used adiabatic indices via

$$c_{\mathrm{s}}^2 = \frac{p\Gamma}{\rho} , \quad \text{and} \quad \mathcal{C}^2 = \frac{p\Gamma_1}{\rho} , \tag{23}$$

where Γ and Γ_1 are the adiabatic indices of the background and perturbed matter, respectively. We also introduce the density scale

height (which is convenient as we want to avoid involving an explicit stellar model in the plane-wave analysis below)

$$\frac{1}{H} = \frac{1}{\rho}\frac{\mathrm{d}\rho}{\mathrm{d}r} . \tag{24}$$

With these definitions, we have

$$\delta p_l = \left[1 + \frac{1}{1 + i\mathcal{A}/\omega_n}\left(\frac{\mathcal{C}^2}{c_{\mathrm{s}}^2} - 1\right)\right]c_{\mathrm{s}}^2\delta\rho_l$$
$$+ \frac{1}{1 + i\mathcal{A}/\omega_n}\left(\frac{\mathcal{C}^2}{c_{\mathrm{s}}^2} - 1\right)c_{\mathrm{s}}^2\left(\frac{\rho W_l}{rH}\right) . \tag{25}$$

When solving the equations numerically later on, we will want to remove $\delta\rho_l$ so we need

$$\delta\rho_l = \left[1 + \frac{1}{1 + i\mathcal{A}/\omega_n}\left(\frac{\mathcal{C}^2}{c_{\mathrm{s}}^2} - 1\right)\right]^{-1}$$
$$\left\{\frac{1}{c_{\mathrm{s}}^2}\delta p_l - \frac{1}{1 + i\mathcal{A}/\omega_n}\left(\frac{\mathcal{C}^2}{c_{\mathrm{s}}^2} - 1\right)\left(\frac{\rho W_l}{rH}\right)\right\} . \tag{26}$$

Finally, we define the Brunt–Väisälä frequency as

$$\mathcal{N}^2 = g^2\left(\frac{1}{c_{\mathrm{s}}^2} - \frac{1}{\mathcal{C}^2}\right) = \frac{c_{\mathrm{s}}^4}{H^2}\left(\frac{1}{c_{\mathrm{s}}^2} - \frac{1}{\mathcal{C}^2}\right)$$
$$= -\frac{c_{\mathrm{s}}^4}{H^2\mathcal{C}^2}\left(1 - \frac{\mathcal{C}^2}{c_{\mathrm{s}}^2}\right) , \tag{27}$$

where the local gravitational acceleration is

$$g = \frac{\mathrm{d}\Phi}{\mathrm{d}r} = -\frac{1}{\rho}\frac{\mathrm{d}p}{\mathrm{d}r} = -\frac{c_{\mathrm{s}}^2}{H} . \tag{28}$$

This leads to

$$\frac{\mathcal{C}^2}{c_{\mathrm{s}}^2} - 1 = \frac{\mathcal{N}^2 H^2 \mathcal{C}^2}{c_{\mathrm{s}}^4} \equiv \bar{\mathcal{N}}^2 , \tag{29}$$

which is the dimensionless Brunt–Väisälä frequency, and we have

$$\delta\rho_l = \left[1 + \frac{\bar{\mathcal{N}}^2}{1 + i\mathcal{A}/\omega_n}\right]^{-1}\left\{\frac{1}{\mathcal{C}_{\mathrm{s}}^2}\delta p_l - \frac{\bar{N}^2}{1 + i\mathcal{A}/\omega_n}\left(\frac{\rho W_l}{rH}\right)\right\} . \tag{30}$$

Finally, rewriting (7) and (10) we get

$$\frac{\mathrm{d}\delta p_l}{\mathrm{d}r} - \frac{c_{\mathrm{s}}^2}{H}\delta\rho_l = \frac{\omega_n^2\rho}{r}W_l - \rho\frac{\mathrm{d}\delta\Phi_l}{\mathrm{d}r} , \tag{31}$$

and

$$\frac{\mathrm{d}(r\rho W_l)}{\mathrm{d}r} = -r^2\delta\rho_l + \frac{l(l+1)}{\omega_n^2}(\rho\delta\Phi_l + \delta p_l) . \tag{32}$$

The last three equations are the main equations that will be used to determine the neutron star g modes.

3 PLANE-WAVE ANALYSIS

In order to gain intuition and help explain the numerical results later, it is useful to consider a local plane-wave analysis.[2] First, we introduce

$$\bar{W}_l = \frac{\rho W_l}{r} , \tag{33}$$

to get the, fairly concise, equations

---

[2]The analysis here is similar to that of Andersson & Pnigouras (2019) but the simplifications we make are less restrictive.

$$\frac{\mathrm{d}\delta p_l}{\mathrm{d}r} - \frac{c_\mathrm{s}^2}{H}\delta\rho_l = \omega_n^2 \bar{W}_l - \rho\frac{\mathrm{d}\delta\Phi_l}{\mathrm{d}r}, \tag{34}$$

$$\frac{\mathrm{d}\left(r^2\bar{W}_l\right)}{\mathrm{d}r} = -r^2\delta\rho_l + \frac{l(l+1)}{\omega_n^2}\left(\rho\delta\Phi_l + \delta p_l\right), \tag{35}$$

and

$$\delta\rho_l = \left[1 + \frac{\bar{\mathcal{N}}^2}{1 + i\mathcal{A}/\omega_n}\right]^{-1}\left\{\frac{1}{c_\mathrm{s}^2}\delta p_l - \frac{\bar{\mathcal{N}}^2}{1 + i\mathcal{A}/\omega_n}\left(\frac{\bar{W}_l}{H}\right)\right\}, \tag{36}$$

From these equations it is evident that the problem will change when we consider finite time–scale reactions. In the limit of no reactions, when $\mathcal{A} = 0$, we are dealing with an eigenvalue problem for ω_n^2, so we will always have two roots $\pm\omega_n$. When $\mathcal{A} \neq 0$ the eigenvalues become complex and the symmetry of the mode pairs is less obvious.

As we are mainly interested in the qualitative behaviour at this point, we introduce the Cowling approximation (which is expected to be reasonably accurate for the g modes); setting $\delta\Phi_l = 0$. Then, using (36) to remove $\delta\rho_l$ from the problem we get

$$\frac{\mathrm{d}\delta p_l}{\mathrm{d}r} - \left[1 + \frac{\bar{\mathcal{N}}^2}{1 + i\mathcal{A}/\omega_n}\right]^{-1}\left(\frac{\delta p_l}{H}\right)$$
$$= \left\{\omega_n^2 - \frac{c_\mathrm{s}^2}{H^2}\left[1 + \frac{\bar{\mathcal{N}}^2}{1 + i\mathcal{A}/\omega_n}\right]^{-1}\frac{\bar{\mathcal{N}}^2}{1 + i\mathcal{A}/\omega_n}\right\}\bar{W}_l, \tag{37}$$

and

$$\frac{1}{r^2}\frac{\mathrm{d}(r^2\bar{W}_l)}{\mathrm{d}r} - \left[1 + \frac{\bar{\mathcal{N}}^2}{1 + i\mathcal{A}/\omega_n}\right]^{-1}\frac{\bar{\mathcal{N}}^2}{1 + i\mathcal{A}/\omega_n}\left(\frac{\bar{W}_l}{H}\right)$$
$$= \left\{\frac{\mathcal{L}_l^2}{\omega_n^2} - \left[1 + \frac{\bar{\mathcal{N}}^2}{1 + i\mathcal{A}/\omega_n}\right]^{-1}\right\}\frac{\delta p_l}{c_\mathrm{s}^2}, \tag{38}$$

where the Lamb frequency is defined as

$$\mathcal{L}_l^2 = \frac{l(l+1)c_\mathrm{s}^2}{r^2}. \tag{39}$$

In order to explore the nature of the waves we are interested in, we now adopt the plane-wave approach with

$$\hat{p} = \delta p_l, \qquad \hat{W} = r^2\bar{W}_l, \qquad \partial_r \to ik. \tag{40}$$

This leads to

$$\left(ik - \left[1 + \frac{\bar{\mathcal{N}}^2}{1 + i\mathcal{A}/\omega_n}\right]^{-1}\frac{1}{H}\right)$$
$$\hat{p} = \left(\omega_n^2 - \left[1 + \frac{\bar{\mathcal{N}}^2}{1 + i\mathcal{A}/\omega_n}\right]^{-1}\frac{\bar{\mathcal{N}}^2 c_\mathrm{s}^2}{1 + i\mathcal{A}/\omega_n}\frac{1}{H^2}\right)\frac{\hat{W}}{r^2}, \tag{41}$$

$$\left(ik - \left[1 + \frac{\bar{\mathcal{N}}^2}{1 + i\mathcal{A}/\omega_n}\right]^{-1}\frac{\bar{\mathcal{N}}^2}{1 + i\mathcal{A}/\omega_n}\frac{1}{H}\right)\frac{\hat{W}}{r^2}$$
$$= \left(\frac{\mathcal{L}_l^2}{\omega_n^2} - \left[1 + \frac{\bar{\mathcal{N}}^2}{1 + i\mathcal{A}/\omega_n}\right]^{-1}\right)\frac{\hat{p}}{c_\mathrm{s}^2}. \tag{42}$$

Here, we make two simplifying assumptions. First, we focus on short-wavelength motion, such that $k|H| \gg 1$. Second, we assume that $\bar{\mathcal{N}}^2 \ll 1$ as appropriate for weakly stratified matter (eventually leading to the anticipated low-frequency g modes).

It is easy to see how the expected barotropic result emerges in the $\mathcal{N}^2 \to 0$ limit. For fast reactions, we get

$$\left(ik - \frac{1}{H}\right)\hat{p} \approx ik\hat{p} = \omega_n^2\frac{\hat{W}}{r^2}, \tag{43}$$

$$ik\frac{\hat{W}}{r^2} = -\left(1 - \frac{\mathcal{L}_l^2}{\omega_n^2}\right)\frac{\hat{p}}{c_\mathrm{s}^2}, \tag{44}$$

leading to the dispersion relation

$$\omega_n^2 = c_\mathrm{s}^2 k^2 + \mathcal{L}_l^2. \tag{45}$$

This solution represents sound waves – the pressure p modes in the full mode calculation later. Higher overtone modes have shorter scales (=larger k) and therefore lie at higher frequencies. In a neutron star, we expect to find an infinite set of high-frequency p modes.

In the opposite limit of slow reactions, we have

$$ik\hat{p} = \left(\omega_n^2 - \frac{\bar{\mathcal{N}}^2 c_\mathrm{s}^2}{H^2}\right)\frac{\hat{W}}{r^2}, \tag{46}$$

$$ik\frac{\hat{W}}{r^2} = -\left(1 - \frac{\mathcal{L}_l^2}{\omega_n^2}\right)\frac{\hat{p}}{c_\mathrm{s}^2}. \tag{47}$$

Now we instead arrive at

$$k^2 c_\mathrm{s}^2 = \left(\omega_n^2 - \frac{\bar{\mathcal{N}}^2 c_\mathrm{s}^2}{H^2}\right)\left(1 - \frac{\mathcal{L}_l^2}{\omega_n^2}\right). \tag{48}$$

This equation has two sets of roots. If it is also the case that (effectively focusing of dynamics slower than the sound waves)

$$\omega_n^2 \ll \mathcal{L}_l^2, \tag{49}$$

then

$$\omega_n^2 \equiv \omega_0^2 \approx \mathcal{N}^2\frac{\mathcal{C}^2}{c_\mathrm{s}^2}\left(\frac{k^2 c_\mathrm{s}^2 + \mathcal{L}_l^2}{\mathcal{L}_l^2}\right)^{-1} \approx \mathcal{N}^2\frac{\mathcal{C}^2}{c_\mathrm{s}^2}\frac{l(l+1)}{k^2 r^2 + l(l+1)}. \tag{50}$$

In the opposite limit, when

$$\omega_n^2 \gg \mathcal{L}_l^2, \tag{51}$$

it is easy to see that we retain the p modes from the barotropic case. In essence, the introduction of the stratification has added a set of low-frequency modes to the spectrum. These are the g modes (Reisenegger & Goldreich 1992). It is easy to see that, as the wavelength decreases (=larger k) the frequency decreases. This agrees with the results of Unno et al. (1989) where in beta equilibrium, the g-mode frequency was shown to tend to

$$\omega_n^2 \approx \frac{\mathcal{N}^2\mathcal{L}_l^2}{c_\mathrm{s}^2 k^2 + \mathcal{L}_l^2}. \tag{52}$$

In a neutron star, with stable stratification, we expect to find an infinite set of undamped, low-frequency g modes. This changes when we consider the nuclear reactions.

For finite reaction rates, we have (again, focussing on the $\omega_n^2 \ll \mathcal{L}_l^2$ case)

$$ik\hat{p} = \left(\omega_n^2 - \frac{\mathcal{N}^2}{1 + i\mathcal{A}/\omega_n}\frac{\mathcal{C}^2}{c_\mathrm{s}^2}\right)\frac{\hat{W}}{r^2}, \tag{53}$$

$$ik\frac{\hat{W}}{r^2} = \frac{\mathcal{L}_l^2}{\omega_n^2}\frac{\hat{p}}{c_\mathrm{s}^2}. \tag{54}$$

That is,

$$\frac{k^2 c_\mathrm{s}^2 + \mathcal{L}_l^2}{\mathcal{L}_l^2} \approx \frac{t_\mathrm{R}}{\omega_n t_\mathrm{R} - i}\frac{\mathcal{C}^2}{c_\mathrm{s}^2}\frac{\mathcal{N}^2}{\omega_n}, \tag{55}$$

or

$$\omega_n \approx \frac{t_\mathrm{R}}{\omega_n t_\mathrm{R} - i}\mathcal{N}^2\frac{\mathcal{C}^2}{c_\mathrm{s}^2}\left(\frac{k^2 c_\mathrm{s}^2 + \mathcal{L}_l^2}{\mathcal{L}_l^2}\right)^{-1} = \frac{t_\mathrm{R}}{\omega_n t_\mathrm{R} - i}\omega_0^2. \tag{56}$$

As expected, the reactions lead to complex-frequency (damped) oscillations. This is as it should be, given that the reactions lead to bulk viscosity which damps the fluid motion (Schmitt & Shternin 2018). It is, however, easy to see that we retain the previous (undamped!) results in the fast/slow reaction limits.

In the general case, solving for the frequency we have

$$\omega_n \approx \frac{1}{2t_R} \left[i \pm \left(4\omega_0^2 t_R^2 - 1 \right)^{1/2} \right]. \tag{57}$$

This is the key result. Taylor expanding for large $\omega_0 t_R$ we see that

$$\omega_n \approx \pm\omega_0 + \frac{i}{2t_R}. \tag{58}$$

That is, the two modes from the non-reactive problem are both damped and symmetric with respect to the imaginary axis. If we consider how the waves propagate on the star (e.g. in terms of the mode pattern speed $\sigma_p = -\omega_n/m$) the pair of solutions can be thought of as travelling in opposite directions around the star. The numerically determined modes (see the following section) retain this symmetry. It is useful to keep this in mind, even though we will, for simplicity, focus mainly on mode frequencies with a positive real part. Similarly, it is easy to see that both roots become purely imaginary in the fast-reaction limit. The two roots then limit to $\omega_n = 0$ and i/t_R (which means that $\omega_n \to i\infty$ as $t_R \to 0$), respectively. In fact, it is easy to see that there are no oscillatory modes below a *critical reaction time–scale*, given by

$$t_R = 1/2\omega_0. \tag{59}$$

This corresponds to the parameters for which (57) has a repeated root and the pair of modes from (58) merge on the imaginary axis. Above the critical reaction time, the modes split again and one of them moves towards the origin while the other moves towards $+i\infty$ as t_R decreases. This will be illustrated later in Fig. 4. In this regime the mode solutions represent pure diffusion. Instead of having a damped oscillatory motion, the fluid simply relaxes towards equilibrium. Above the critical time–scale, for larger values of t_R, we have damped oscillations. The implications of this behaviour are – at least formally – important. While the classic analysis suggests that the g-mode spectrum is infinite, for a realistic neutron star model this cannot be so. The (potentially very) high overtones, for which $\omega_0 t_R$ is small, will be overdamped. This accords with the results of the toy model from Andersson & Pnigouras (2019).

Finally, from (57) we see that, in the regime where the modes are oscillatory, we have $\omega_n^2 \approx \omega_0^2$. In essence, we expect the modes to move along a quarter circle, from the real axis (when $t_R = \infty$) to the imaginary axis (at the critical reaction time). This is shown later in Fig. 3. This prediction is testable with numerical solutions and we now turn to that problem.

4 NUMERICAL RESULTS

4.1 Dimensionless form

In order to solve the mode equations numerically, it is convenient to work with a dimensionless formulation (Unno et al. 1989). Relaxing the Cowling approximation, we define the following variables,

$$y_1 = \frac{W_l}{r^2}, \tag{60}$$

$$y_2 = \frac{1}{gr} \left(\frac{\delta p_l}{\rho} + \delta\Phi_l \right), \tag{61}$$

$$y_3 = \frac{1}{gr} \delta\Phi_l, \tag{62}$$

$$y_4 = \frac{1}{g} \frac{d\delta\Phi_l}{dr}. \tag{63}$$

Inserting these definitions into (30)–(32) and the perturbed Poisson equation (11) we arrive at the coupled differential equations

$$r\frac{dy_1}{dr} = \left(-\frac{d\ln\rho}{d\ln r} - 3 \right) y_1 + \frac{l(l+1)}{\tilde{\omega}_n^2 c_1} y_2 - \left[1 + \frac{\bar{\mathcal{N}}^2}{1 + i\mathcal{A}/\omega_n} \right]^{-1}$$
$$\times \left\{ \frac{1}{c_s^2} gr(y_2 - y_3) - \frac{\bar{\mathcal{N}}^2}{1 + i\mathcal{A}/\omega_n} \left(\frac{ry_1}{H} \right) \right\}, \tag{64}$$

$$r\frac{dy_2}{dr} = \tilde{\omega}_n^2 c_1 y_1 - \left[1 + \frac{d\ln(\rho g)}{d\ln r} \right] y_2 + \frac{d\ln\rho}{d\ln r} y_3$$
$$+ \left[1 + \frac{\bar{\mathcal{N}}^2}{1 + i\mathcal{A}/\omega_n} \right]^{-1}$$
$$\times \left\{ \frac{r}{H}(y_2 - y_3) - \frac{\bar{\mathcal{N}}^2}{1 + i\mathcal{A}/\omega_n} \frac{c_s^2}{H^2} \left(\frac{ry_1}{g} \right) \right\}, \tag{65}$$

$$r\frac{dy_3}{dr} = (1 - U)y_3 + y_4, \tag{66}$$

and

$$r\frac{dy_4}{dr} = l(l+1)y_3 - Uy_4 + 4\pi G\rho \left[1 + \frac{\bar{\mathcal{N}}^2}{1 + i\mathcal{A}/\omega_n} \right]^{-1}$$
$$\times \left\{ \frac{1}{c_s^2} r^2(y_2 - y_3) - \frac{\bar{\mathcal{N}}^2}{1 + i\mathcal{A}/\omega_n} \left(\frac{r^2 y_1}{gH} \right) \right\}. \tag{67}$$

The equation for y_3 is obtained from the trivial relationship between y_3 and y_4 and we have the used the same definitions as Unno et al. (1989) where

$$\tilde{\omega}_n^2 = \frac{\omega_n^2}{GM/R^3}, \tag{68}$$

$$c_1 = \left(\frac{r}{R} \right)^3 \frac{M}{m}, \tag{69}$$

$$m = \int_0^r 4\pi\rho r^2 \, dr \tag{70}$$

$$U = 2 + \frac{d\ln g}{d\ln r} = \frac{4\pi\rho r^3}{m}. \tag{71}$$

We also define

$$Z = -\frac{d\ln\rho}{d\ln r} = -\frac{r}{H}, \tag{72}$$

and let M and R be the total mass and radius of the background star, respectively. Using (28) we can rewrite the equations as

$$x\frac{dy_1}{dx} = (Z - 3)y_1 + \frac{l(l+1)}{\tilde{\omega}_n^2 c_1} y_2 - Z \left[1 + \frac{\bar{\mathcal{N}}^2}{1 + i\mathcal{A}/\omega_n} \right]^{-1}$$
$$\times \left\{ y_2 - y_3 + \frac{\bar{\mathcal{N}}^2}{1 + i\mathcal{A}/\omega_n} y_1 \right\}, \tag{73}$$

$$x\frac{dy_2}{dx} = \tilde{\omega}_n^2 c_1 y_1 + (Z - U + 1)y_2 - Zy_3 - Z \left[1 + \frac{\bar{\mathcal{N}}^2}{1 + i\mathcal{A}/\omega_n} \right]^{-1}$$
$$\times \left\{ y_2 - y_3 + \frac{\bar{\mathcal{N}}^2}{1 + i\mathcal{A}/\omega_n} y_1 \right\}, \tag{74}$$

$$x\frac{dy_3}{dx} = (1 - U)y_3 + y_4, \tag{75}$$

$$x\frac{dy_4}{dx} = l(l+1)y_3 - Uy_4 + UZ \left[1 + \frac{\bar{\mathcal{N}}^2}{1 + i\mathcal{A}/\omega_n} \right]^{-1}$$
$$\times \left\{ y_2 - y_3 + \frac{\bar{\mathcal{N}}^2}{1 + i\mathcal{A}/\omega_n} y_1 \right\}, \tag{76}$$

where

$$x = \frac{r}{R}, \tag{77}$$

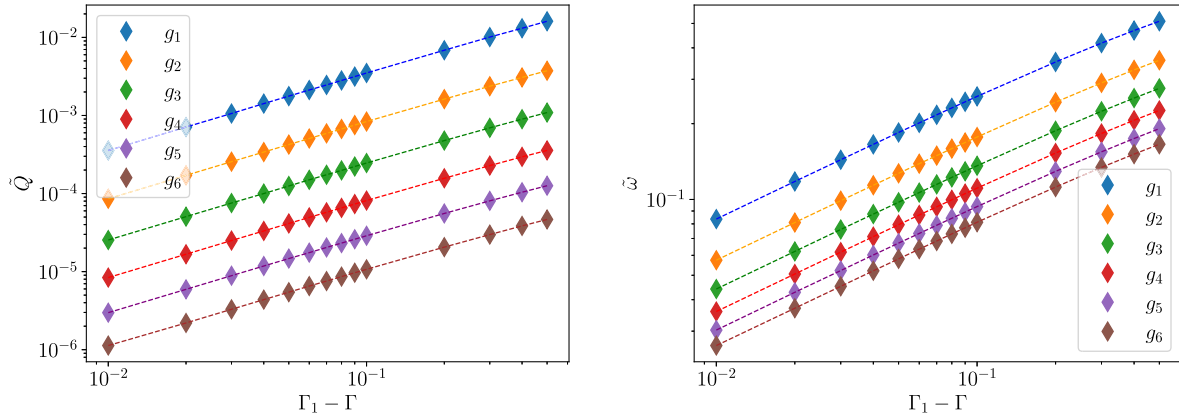is a dimensionless radial coordinate. This system of equation can be

Figure 1. Plots of the dimensionless overlap integral $\tilde{Q}_n$ (left panel) and dimensionless frequencies $\tilde{\omega}$ (right panel) against the difference $\Gamma_1 - \Gamma$ on log–log scales for the first six g modes. The background star is polytropic with $\gamma = 2$, $R = 10$ km, and $M = 1.4\,M_\odot$. For the overlap integrals the slopes range from $0.95 - 0.98$ and for the frequencies the slopes range from $0.46 - 0.47$.

compared to that used by, for example, Unno et al. (1989) and it is easy to confirm that our set limits to the usual one when $\mathcal{A} \to 0$.

Next we need four boundary conditions: two regularity conditions at the centre of the star and two conditions at the surface. Near the origin, as $r \to 0$, a Taylor expansion reveals that the we should have

$$c_1 \tilde{\omega}_n^2 y_1 - l y_2 = 0, \tag{78}$$

and

$$l y_3 - y_4 = 0. \tag{79}$$

Meanwhile, near the star's surface, as $r \to R$, we need to impose the vanishing of the Lagrangian pressure perturbation and the continuity of the gravitational potential and its derivative. These conditions take the form

$$(l + 1) y_3 + y_4 = 0, \tag{80}$$

and

$$y_1 - y_2 + y_3 = 0. \tag{81}$$

These relations follow by requiring that $\delta\Phi_l$ vanishes at infinity and that there exists a distinct boundary of the star where $\rho, p \approx 0$, thus $\Delta p = 0$. These are the same boundary conditions as in the usual calculation (Unno et al. 1989). We also note that our equations have no dependence on m which is to be expected due to the spherical symmetry of the background star. Finally, to close the system we need an equation of state. We will discuss our chosen model below.

4.2 Results

First of all, in order to gain confidence in the numerical implementation, we reproduce (and check) relevant results from the literature. The natural choice is to consider a $\Gamma = 2$ ($n = 1$) polytrope with a constant Γ_1 representing the stratification, see for example Pnigouras (2017). More recent work by Xu & Lai (2017), shows that the numerical results for polytropic stars follow particular scaling relations. In particular,

$$\tilde{\omega}_n \propto (\Gamma_1 - \Gamma)^{1/2}, \tag{82}$$

and

$$\tilde{Q}_n \propto \Gamma_1 - \Gamma, \tag{83}$$

where $\tilde{Q}_n$ is the dimensionless overlap integral defined as

$$\tilde{Q}_n = \frac{1}{MR^l} \int_0^R \delta\rho_l r^{l+2} \, dr, \tag{84}$$

commonly referred to as the mass-multipole moment of each respective mode.

Using the results from our code we obtain the results shown in Fig. 1 for the first six g modes, where $\Gamma = 2$ and Γ_1 is varied from $2.01 - 2.5$. This allows us to confirm the suggested scaling relations. Using a linear regression function, for the overlap integrals the slopes range from $0.95 - 0.98$ and for the frequencies the slopes range from $0.46 - 0.47$. This is in agreement with (82)–(83) allowing for small numerical errors.

4.3 Realistic stratification

In order to make the model more realistic we introduce stratification motivated by the BSk family of equations of state (Fantina et al. 2013; Potekhin et al. 2013). Specifically, mainly as proof of principle, we provide results for the BSk21 model (see also Andersson & Gittins 2023; Gittins & Andersson 2023). First, from BSk21 table, the relationship $p(n_b)$ and $\bar{\mathcal{N}}^2(n_b)$ are calculated, where n_b is the baryon number density. From this, n_b is converted to mass density using $\rho = m_b n_b$, where m_b is baryon mass. The pressure and density profiles as function of radius then follow (as usual) from the Newtonian stellar structure equations. Having fixed the equation of state, we still need to pick a sample neutron star. The particular model we consider has central density $\rho = 5.10 \times 10^{15}\,\mathrm{g\,cm^{-3}}$, which leads to a radius of $R = 13.49$ km and a mass of $M = 1.43\,M_\odot$. Equations (73)–(76) along with the boundary conditions (78)–(81) were solved numerically using this background star and for different reaction rates by varying $\mathcal{A}$.

From the behaviour of the radial eigenfunction, $W_l(r)$, and the mode-frequency we determine if a mode is a p or g mode. Gravity modes tend to have small ω_n and a $W_l(r)$ that shows prominent features well beneath the surface of the star. Meanwhile, p modes will have higher ω_n and a $W_l(r)$ that shows prominent features close to the surface. The fundamental f mode can be thought of as the p mode with the lowest frequency. One can also easily distinguish between overtones of the p and g modes. As the overtone n increases, ω_n will decrease for g modes but increase for p modes (as per the plane-wave discussion). Also by examining $W_l(r)$ again, the number of nodes in the diagram is roughly equal to n, allowing us to identify
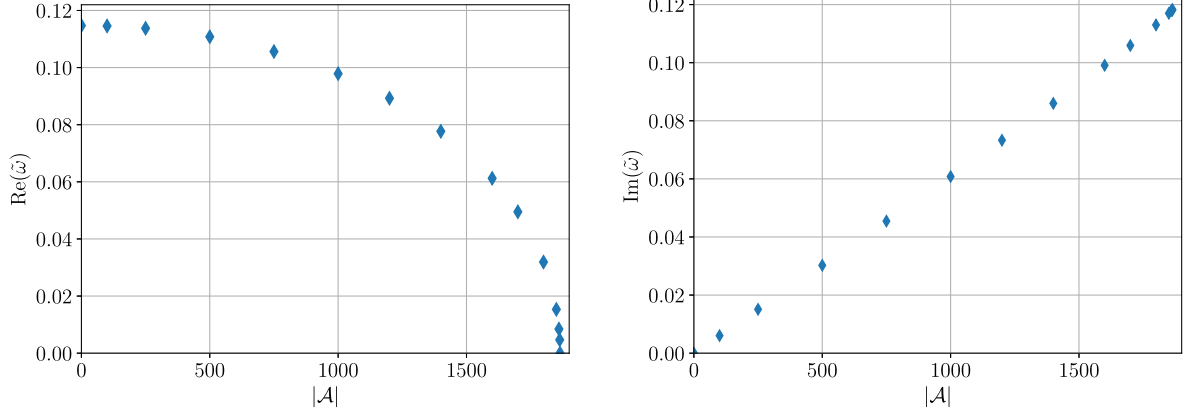
Figure 2. Plots showing how the dimensionless mode frequency of the fundamental g mode, g_1, varies with $\mathcal{A}$. Plotted separately are the real and imaginary parts of the frequency on the left and right, respectively.
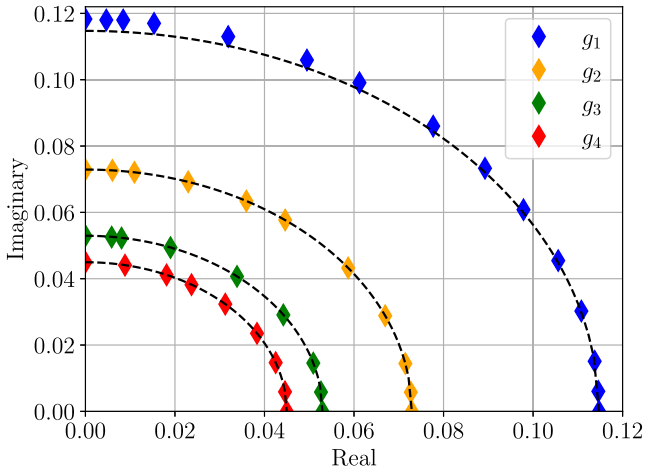
Figure 3. Results showing how the dimensionless frequencies $\tilde{\omega}_n$ of the first four g modes ($g_1 - g_4$) move in the complex plane when the reaction rate is varied. The diamonds represent the numerical values and the dashed lines represent the theoretical prediction of a circle with a radius equal to the numerical value of the g-mode frequency when $\mathcal{A} \approx 0$.
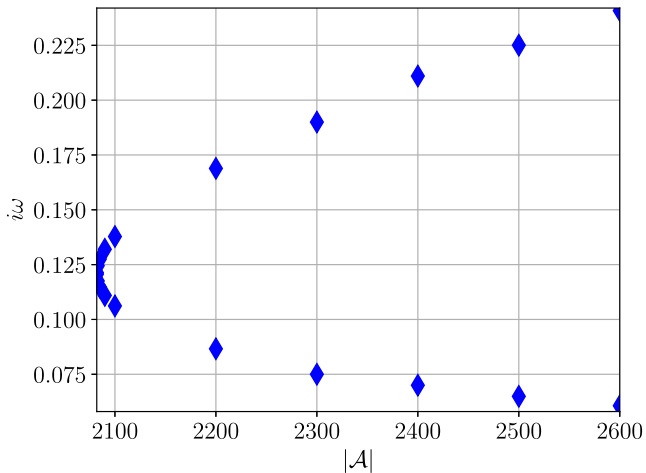
Figure 4. Plot of the pair of g_1 modes with purely imaginary frequencies beyond the critical reaction time, for different values of $\mathcal{A}$.

the specific overtones. In the figures and tables below we only show results for the g modes as they depend the most sensitively on the reactions.

For slow reaction rates, $t_r > 1\,\mathrm{s}$ in the illustrated case, the modes exhibit minuscule damping, $\mathrm{Re}(\omega) \gg \mathrm{Im}(\omega) \approx 0$. The expected modes are found; the f mode and the g and p modes with their respective overtones. When $t_r < 1\mathrm{s}$, the damping begins to increase for all modes. As expected, the effect is greater for the g modes due to their relatively low frequencies in comparison to the f and p modes. As can be seen in Fig. 2, as $|\mathcal{A}|$ increases, which corresponds to $t_r \to 0$, the real part of the mode frequency decreases while the imaginary part increases. However, the magnitude of the oscillation frequency remains constant and can be seen in Fig. 3, where the mode frequency has been plotted for the first four g-modes.

Beyond the critical reaction rate from (59), a pair of pure imaginary modes are found for each specific g mode, g_n. As the reaction rate becomes faster, the pair diverge, both staying on the imaginary axis but one increasing and the other tending towards the origin. This is illustrated for the specific case of g_1 in Fig. 4, but the same behaviour is exhibited by all other g modes we have considered. The result agrees with the expectations from the plane-wave analysis of the fast reaction limit, so we are confident that it is robust.

As expected, the lowest frequency g modes are the first to hit their critical reaction rate and reach the imaginary axis. In agreement with the plane wave argument, we see that the frequency at which the g modes first hit the imaginary axis is approximately the imaginary counterpoint of the real-valued g-mode frequencies in the slow reaction limit. Sample numerical data showing this are provided in Table 1, in good agreement with the predicted behaviour in the fast reaction limit. We also see that, as the g modes sweep through the complex plane they appear to trace a circular path, with centre at the origin and radius of the initial slow-reaction limit mode frequency. The solution with a negative real part traces a symmetric pattern in the second quadrant of the complex plane. Once the g modes hit the imaginary axis, the symmetry breaks and the two mode solutions diverge along the imaginary axis, as previously discussed.

5 CONCLUSIONS

Expanding on the work of Andersson & Pnigouras (2019) we have shown how the presence of nuclear reactions in a neutron star leads to a damping of the composition g modes for arbitrary reaction rates.

Table 1. Dimensionless frequencies of the first ten g modes, calculated numerically for $\mathcal{A} = 0$ and for when the mode frequency first becomes purely imaginary which we will call the critical frequency, $\mathcal{A}_{\mathrm{crit}}$. The ratio is defined as $\frac{|\mathcal{A}_{\mathrm{crit}}|}{Im(\omega_{\mathcal{A}=0})}$. As we can see this agrees well with the predicted value of 2 from (59).

Mode	$\tilde{\omega}_{\mathcal{A}=0}$	$\tilde{\omega}_{\mathcal{A}_{\mathrm{crit}}}$	$|\mathcal{A}_{\mathrm{crit}}|$	Ratio
g_1	0.115	0.118i	1864.2	1.84
g_2	0.0729	0.0729i	1264.3	1.97
g_3	0.0529	0.0529i	910.6	1.95
g_4	0.0450	0.0450i	764.9	1.93
g_5	0.0380	0.0380i	649.2	1.94
g_6	0.0328	0.0328i	560.4	1.94
g_7	0.0288	0.0288i	491.5	1.94
g_8	0.0257	0.0257i	438.1	1.94
g_9	0.0232	0.0231i	395.3	1.94
g_{10}	0.0211	0.0211i	359.9	1.94

We have extended the proof-of-principle work to an actual stellar model based on a realistic matter composition (based on the BSk21 equation of state) and incorporating the relevant mode boundary conditions. This was achieved by setting up linear perturbation equations in a dimensionless formalism similar to that of Unno et al. (1989) and others. We showed that, as the reaction rate increases, the mode frequencies sweep through the complex plane from the real axis to the imaginary axis. As a consequence, the higher order modes are the first to be removed from the oscillation spectrum. This continues until, at a certain reaction rate, there would be no oscillatory g modes left in the neutron star. The good agreement between our numerical results and those derived from our plane-wave analysis provides strong confidence in these conclusions.

While we have only demonstrated the concept for a specific equation of state and a single background neutron star, the results serve as an important proof of principle. Qualitatively, the results should extend other equation of state models. Quantitatively, changing the equation of state (and hence the matter composition variation) and varying parameters such as the mass and radius of the star would obviously affect the specific mode frequencies. However, the close agreement with the local plane-wave analysis strongly suggest that the collective behaviour and trends we have identified should be universal.

The results we provide may not have immediate implications for most astrophysical applications – realistic nuclear reactions tend to be very slow compared to the oscillation time–scale of the low-order g modes, so we need to consider very high-order modes in order for the reactions to play a dominant role – but three relevant problems immediately come to mind. First, the non-linear saturation of mode driven unstable by gravitational-wave emission is effected by the coupling to higher order pressure p modes and gravity g modes (Schenk et al. 2001; Pnigouras & Kokkotas 2015). The nature of the higher order modes clearly impacts on the result. Second, the so-called p–g instability, which has been proposed to operate in neutron star binaries (Weinberg, Arras & Burkart 2013), involves the (supposedly) non-resonant coupling of very high-order p modes and g modes to the dynamical tide. The presence (or absence) of the instability depends on the spectrum of high-order g modes. Finally, still in the context of dynamical tides, the mode-sum decomposition that is used to describe the dynamical tide in a binary system (and Newtonian gravity) assumes that the mode problem is Hermitian (Pnigouras et al. 2024). If that is not so, e.g. if we account for bulk viscosity damping associated with nuclear reactions, then one might have to rethink the formal validity

of the standard argument. In essence, while the low-order modes are likely to be the most relevant from an observational point of view, there are good reasons to explore the high-order g-mode spectrum.

Following on from these results, the next step would be to consider more realistic background stars by extending this calculation to general relativity. One could also consider the impact temperature profiles and gradients would have on the g modes. For example, work by Krüger, Ho & Andersson (2015) shows that the g-mode frequencies and damping times can be dramatically affected by high temperatures. Finite temperatures also bring in a new class of g modes, thermal g modes, in addition to the composition modes we have considered here. This future direction would open the way to considering objects like proto-neutron stars formed after the gravitational collapse of successful core-collapse supernova explosions (Ferrari, Miniutti & Pons 2003; Vartanyan et al. 2023), systems where nuclear reactions will also have an impact on the dynamics.

DATA AVAILABILITY

Additional data related to this article will be shared on reasonable request to the corresponding author.

REFERENCES

Abbott B. P., Abbott R., Abbott T. D., Acernese F., Ackley K., Adams C., 2017, Phys. Rev. Lett., 119, 161101

Abbott B. P., Abbott R., Abbott T. D., Acernese F., Ackley K., Adams C., 2018, Phys. Rev. Lett., 121, 161101

Andersson N., Gittins F., 2023, ApJ, 945, 139

Andersson N., Ho W. C. G., 2018, Phys. Rev. D, 97, 023016

Andersson N., Pnigouras P., 2019, MNRAS, 489, 4043

Cowling T. G., 1941, MNRAS, 101, 367

Cox J. P., 1980, Theory of Stellar Pulsation (PSA-2), Vol. 2. Princeton University Press, Princeton

Fantina A. F., Chamel N., Pearson J. M., Goriely S., 2013, A&A, 559, A128

Ferrari V., Miniutti G., Pons J. A., 2003, MNRAS, 342, 629

Finn L. S., 1986, MNRAS, 222, 393

Gittins F., Andersson N., 2023, MNRAS, 521, 3043

Haensel P., Levenfish K. P., Yakovlev D. G., 2002, A&A, 394, 213

Ho W. C. G., Andersson N., 2023, Phys. Rev. D, 108, 043003

Kantor E. M., Gusakov M. E., 2014, MNRAS, 442, L90

Krüger C. J., Ho W. C. G., Andersson N., 2015, Phys. Rev. D, 92, 063009

McDermott P. N., van Horn H. M., Scholl J. F., 1983, ApJ, 268, 837

Miniutti G., Pons J. A., Berti E., Gualtieri L., Ferrari V., 2003, MNRAS, 338, 389

Passamonti A., Andersson N., Pnigouras P., 2022, MNRAS, 514, 1494

Pnigouras P., 2017, PhD thesis, U. Tubingen,

Pnigouras P., Kokkotas K. D., 2015, Phys. Rev. D, 92, 084018

Pnigouras P., Gittins F., Nanda A., Andersson N., Jones D. I., 2024, MNRAS, 527, 8409

Potekhin A. Y., Fantina A. F., Chamel N., Pearson J. M., Goriely S., 2013, A&A, 560, A48

Reisenegger A., Goldreich P., 1992, ApJ, 395, 240

Schenk A. K., Arras P., Flanagan É. É., Teukolsky S. A., Wasserman I., 2001, Phys. Rev. D, 65, 024001

Schmitt A., Shternin P., 2018, in Rezzolla L., Pizzochero P., Jones D. I., Rea N., Vidaña I.eds, The Physics and Astrophysics of Neutron

Stars, Vol. 457, Astrophysics and Space Science Library. Springer Nature Switzerland AG, Cham, Switzerland, p. 455

Unno W., Osaki Y., Ando H., Saio H., Shibahashi H., 1989, Nonradial Oscillations of Stars. Tokyo University Press, Tokyo

Vartanyan D., Burrows A., Wang T., Coleman M. S. B., White C. J., 2023, Phys. Rev. D, 107, 103015

Weinberg N. N., Arras P., Burkart J., 2013, ApJ, 769, 121

Xu W., Lai D., 2017, Phys. Rev. D, 96, 083005

This paper has been typeset from a TeX/LaTeX file prepared by the author.